Solar Energy Materials & Solar Cells 93 (2009) 1986–1993

Contents lists available at ScienceDirect

Solar Energy Materials & Solar Cells

journal homepage: www.elsevier.com/locate/solmat

Investigation of unusual shunting behavior due to phototransistor effect in *n*-type aluminum-alloyed rear junction solar cells

Adeline Sugianto *, Budi S. Tjahjono, Ly Mai, Stuart R. Wenham

Centre of Excellence for Advanced Silicon Photovoltaics and Photonics, University of New South Wales, Sydney NSW 2052, Australia

ARTICLE INFO

Article history:
Received 14 April 2009
Received in revised form
21 July 2009
Accepted 22 July 2009
Available online 15 August 2009

Keywords:
N-type silicon solar cells
Aluminum-alloyed rear junction
Laser doping
Phototransistors
Shunting effect
Schottky contacts

ABSTRACT

N-type silicon wafers have been found to offer numerous advantages over *p*-type silicon wafers, such that they are becoming more widely used for manufacturing high-efficiency commercial solar cells. This paper focuses on work done on *n*-type cell structures with a screen-printed aluminum-alloyed rear junction, laser-doped selective emitter and light-induced plated front contacts to suit large-scale commercial production. However, with such a cell structure we report unusual linear shunting behavior that is only present under illumination but disappears under dark conditions. It was shown that such a phenomenon can be represented by a phototransistor model. In fact, such shunting effects are found to have detrimental impacts on the cell short-circuit current density (J_{sc}) and fill factor (*FF*), which limits the efficiency of cells in this work to 12%.

1. Introduction

N-type silicon potentially allows higher cell performance when compared to equivalent *p*-type silicon due to: (1) smaller capture cross sections of metallic impurities and hence higher bulk lifetime; (2) the absence of light-induced degradation problems with regards to boron–oxygen complexes and (3) better tolerance to high temperature processing [1,2]. Such advantages make the use of cheaper substrates such as Czochralski (CZ) wafers possible, without corresponding loss of device efficiency when compared to equivalent Float Zone wafers. Both these technical and economical advantages have triggered more research on the use of *n*-type silicon wafers, mainly as an alternative base material for the development of various high efficiency commercial cell structures.

In recent years, several techniques have been developed to create the p^+ layer for the emitter formation: (1) boron-diffused emitters; (2) aluminum-alloyed emitters and (3) *p*-type/*i*-type amorphous silicon hetero-junctions. The aluminum-alloyed emitter technique, in particular, is appealing to large-scale cell manufacturing due to the use of well-established screen printing techniques. In this method, both the *p*–*n* junction and the rear metal contact are simultaneously formed at the rear surface following the firing of the aluminum paste. The highest efficiency result on *n*-type large area solar cells with screen-printed aluminum-alloyed rear emitter and screen-printed silver front contacts has been reported to date by Mihailetchi et al. (17.4%) [3], followed by Schmiga et al. (17%) [4].

The *n*-type rear junction cell structure used in this work is designed to both achieve high cell efficiency and make use of simple, fast and low-cost processes that are suitable for large-scale production. In order to meet such requirements, there are three main techniques used in the device fabrication: (1) screen-printing and firing to form a continuous aluminum-alloyed rear junction; (2) laser doping technique to form selective front surface field (FSF) at the front surface; combined with (3) self-aligned metallization as an alternative to screen-printing silver front contacts [5,6]. In particular, a light-induced plating (LIP) technique is used as the preferred self-aligned metallization scheme when compared to electroless plating. This is because LIP offers a significantly faster plating rate that makes it possible to use an inline system and high throughput. Note that the use of front phosphorus-diffused n^+ layer as an FSF layer is left optional to save an additional high-temperature diffusion step. The overall cell structure is illustrated in Fig. 1. Conversion efficiency of 18.6% has been successfully achieved on this cell structure with the presence of the FSF layer [7].

In addition to the abovementioned high efficiency features and the simple, fast fabrication methods, such a cell structure potentially offers a high degree of reliability and hence ensures high yields. This cell structure is, in fact, tolerant of shunting mechanisms that is often caused by plating onto: (1) cell edges and (2) laser-induced defects that expose the bulk. In the former case, it is unlikely that the metal will plate onto the entire cell

* Corresponding author. Tel.: +61 2 93855246; fax: +61 2 93857762.
E-mail addresses: adeline.sugianto@gmail.com (A. Sugianto), s.wenham@unsw.edu.au (S.R. Wenham).

0927-0248/$ - see front matter © 2009 Elsevier B.V. All rights reserved.
doi:10.1016/j.solmat.2009.07.018

edges and introduce a shunting path by electrically connecting the front and rear metal contacts. This is because in LIP the nickel and copper ions plate only onto regions of negative potential [8]. None of the metal ions would therefore plate onto the *p*-type region. Occasionally, the deposited SiN_x layer also wraps around the cell edges and prevents plating in these regions in the first place. In the latter case, the junction is now located at the rear surface. Therefore, following metallization, any laser-induced defects on the side of the laser-doped lines at the front surface would not introduce any shunting paths through or bypassing the *p–n* junction [9].

However, in some cases the light *J–V* measurement indicates strong linear shunting of the cells, which cannot be interpreted in the frame of commonly accepted shunting mechanisms mentioned previously. Interestingly, the observed shunting mechanism is not revealed in dark *J–V* and *Suns–*V_{oc} measurements. Breitenstein and Rakotoniaina [10] observed similar phenomenon through the appearance of unusual lock-in thermography (LIT) signals, whereby bright spots appeared in illuminated LIT images under short-circuit conditions (J_{sc}-ILIT) but were not visible under dark LIT (DLIT). According to Breitenstein and Rakotoniaina, the unsual LIT signals are interpreted to be local Schottky contacts between the metal fingers and the emitter. However, it was not mentioned whether such signals could further correspond to unusual shunting effects in the cells. Therefore, this paper aims to further investigate the presence of the unusual shunting behavior that occurs in the *n*-type rear junction cell structure (Fig. 1), and to study its origin. In addition, this paper also aims to explain on the unusual shunting effect by analyzing its influence on the cell V_{oc}, J_{sc} and *FF*.

2. Detection of unusual shunting behavior

2.1. Experimental details

Two batches of CZ, 1 Ω cm, 〈1 0 0〉 *n*-type silicon wafers were saw-damage-etched and alkaline-textured, resulting in final wafer thicknesses of 200 μm. One batch (Batch 1) underwent front phosphorus diffusion to form an FSF layer (200 Ω/sq), and the residual n^+ layer at the side and rear surface were removed by chemical etch. The other batch (Batch 2) remained undiffused. Both batches then received a standard SiN_x deposition (75 nm thick, refractive index of 2.0) at the front surface. Following the deposition, aluminum paste was screen-printed onto the entire rear surface, followed by spike firing in a belt furnace at 900 °C for 3 s. A coating layer of phosphoric acid 85% was applied to the front surface by spinning method at 3000 rpm for 20 s. The front surface was then scribed using a 532 nm laser with pulsing frequency of 100 kHz and stage speed of 10 mm/s to form a heavily doped selective emitter, which also acts as an opening in the dielectric for the front metal contact pattern. According to the 4-point-probe measurement, the average sheet resistance values of the laser-doped region were 7 Ω/sq and 15 Ω/sq for wafers with and without an FSF, respectively. The front contact metallization was finally carried out by nickel/copper LIP. The copper plating was performed for over 30 min to give adequate thickness of copper.

Cells were then characterized using: (1) light and dark *J–V* measurements to identify the presence of the shunts and (2) DLIT technique to investigate the exact location of the shunts should there be any. In this paper, cell WFSF-6 and NFSF-1 are chosen to

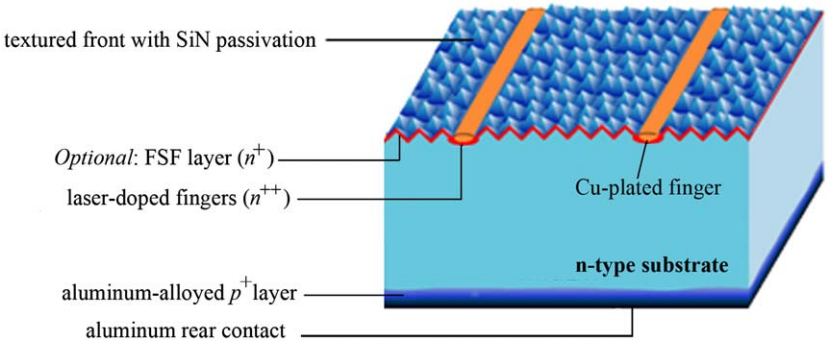

Fig. 1. Schematic cross section of an *n*-type aluminum-alloyed rear junction cell with laser-doped front contacts.

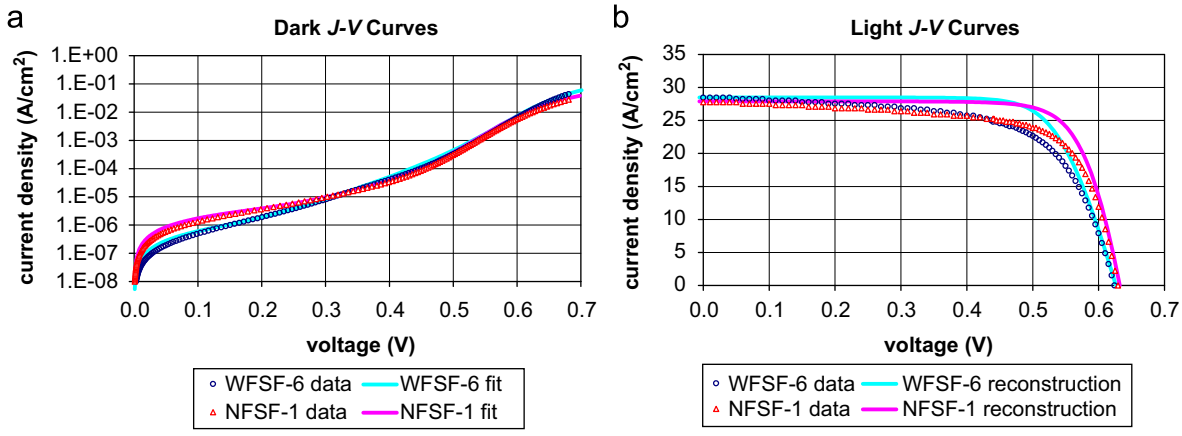

Fig. 2. (a) Measured dark *J–V* curves and their attempted fits, and (b) measured light *J–V* curves and the reconstructed light *J–V* curves from the fitted dark *J–V* curves for WFSF-6 and NFSF-1.

represent each group of cells 'with' and 'without an FSF', respectively.

2.2. Results and discussions

2.2.1. Light and dark J–V measurements

As seen in Fig. 2a, the dark current density J_{dark} for both samples WFSF-6 and NFSF-1 does not show a rapid increase at low voltages but rises in a fairly logarithmic manner. Meanwhile, the measured light J–V curves in Fig. 2b show clear evidence of linear shunting whereby steep slopes are observed at low voltages.

To provide more explanations on the cell characteristics based on the dark and light J–V curve, the measured dark J–V data was theoretically fitted using the two-diode model in Fig. 3. The fitted values under the dark conditions, such as dark saturation current densities (J_{01} and J_{02}), were used to reconstruct the light J–V curves as shown in Fig. 2b, assuming that: (1) the J_{sc} equals to the light generated current J_L for now and (2) for simplicity, J_{01} and J_{02} remain constant both in the dark and under illumination. Different series resistance values are applied for the dark and illuminated conditions due to the different paths of current flow [11]. It is interesting to see from the theoretical fitting that the shape of the dark J–V curve (Fig. 2a) corresponds to cell results with no linear shunts, as confirmed by the corresponding reconstructed light J–V curves (Fig. 2b). Such findings, therefore, contradict the measured data where linear shunting seemingly exists for the same dark J–V curve. It is therefore concluded that unusual linear shunts are observed in both samples. It appears that such shunts only exist under illumination, and hence they cannot be represented by the conventional shunt resistance R_{sh} in the two-diode model.

2.2.2. DLIT measurements

The LIT imaging in this study utilizes Titanium 560 M camera manufactured by Cedip with noise equivalent temperature difference of <25 mK at 25 °C. Fig. 4 shows LIT images for WFSF-6 under reverse-bias (RB) condition at −2 V with signal frequency of 18 Hz. Images were independently taken in the dark and under constant illumination of an external light source at ~0.35 Suns. The constant light source used in this study comprises halogen lights with dichroic filters to approximately simulate the sun's spectrum. In reality, the spectrum peaks within the range of approximately 650–950 nm. Note that the amount of light intensity being received by the sample (0.35 Suns) is limited by the fixed settings of the light source. Regardless, this intensity level is later shown to be adequate for the purpose of this experimentation.

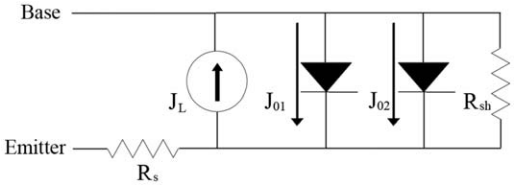

Fig. 3. The two-diode model.

In the DLIT technique, any bright spots normally correspond to shunts or Joule heating [12]. No signs of hotspot heating were observed for the DLIT image in Fig. 4b, while strong LIT signals appeared when the same LIT measurement was repeated under constant illumination from an external halogen light source at ~0.35 Suns (Fig. 4c). Such results are strongly in agreement with the findings in Fig. 3 that (1) the shunting effect occurs only under illumination and it completely disappears in the dark and (2) the shunts are linear. Should such linear shunts exist, the only path that the current can flow in RB is through the shunt resistance R_{sh} while the remaining diodes are reverse-biased (Fig. 3). In addition, these results have also shown that illumination under 0.35 Suns is sufficient for the shunting to be clearly observed. Our later work concludes that higher light intensities would only exacerbate the shunting effect.

The LIT measurement in Fig. 4c also shows that the shunts are localized. The shunts appeared to be located in the effective cell area instead of wrapping around the cell edges, which would otherwise introduce the typical case of shunting that is detected both in the dark and under illumination. By comparing Fig. 4a and c, it can be seen that the shunts originate from the cell area where discontinuities are observed in the front plated metal fingers, as indicated by the circle. Fig. 5 clarifies that discontinuities occur when the copper does not plate uniformly across the finger, typically with the middle part being left unplated. The copper tends to nucleate on the side of the laser-doped area where defects typically occur due to the use of a Gaussian shape for the laser beam (Fig. 5b) [13]. It is highly likely that the laser-induced defects or damage to the SiN_x masking layer exposes the *n*-type bulk when no FSF or a lightly diffused FSF layer (200 Ω/sq) exists. Since the *n*-type bulk is lightly doped (doping concentration $= 5 \times 10^{15}\,cm^{-3}$), any metal that plates onto these defects would form a Schottky type of contact.

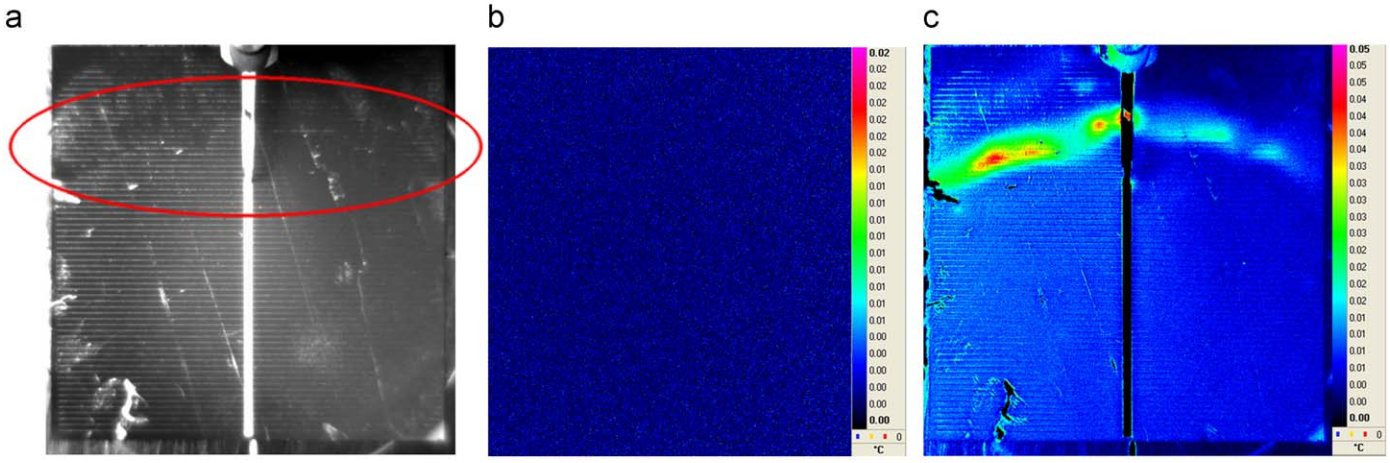

Fig. 4. Different LIT images for WFSF-6: (a) camera image, (b) DLIT image taken and (c) LIT image under steady-state illumination of a halogen light source at ~0.35 Suns. Images were taken at $f = 18$ Hz and $V_{RB} = -2$ V.

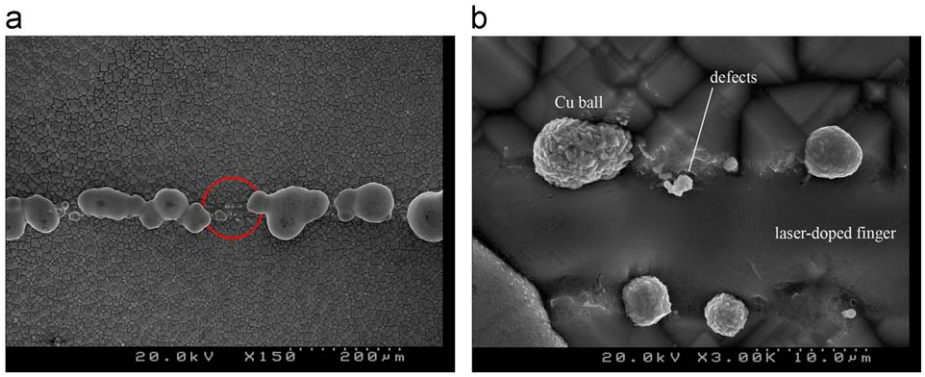

Fig. 5. (a) Laser-doped finger of WFSF-6 that is not fully plated even after over 30-min plating, and hence it gives rise to the unusual shunting effect; (b) close-up picture of the circled area in Fig. 5a: copper balls plate onto the defects that were generated due to non-optimum laser parameters.

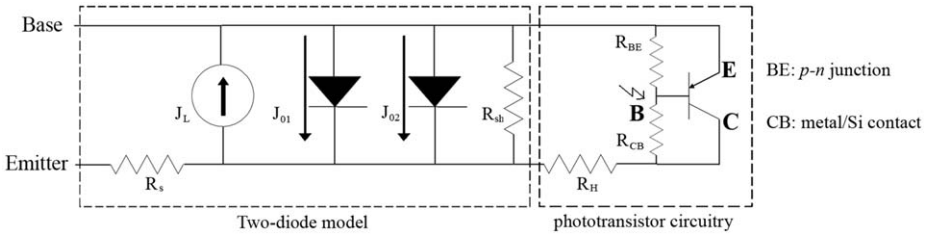

Fig. 6. The two-diode model of a solar cell with an additional phototransistor structure.

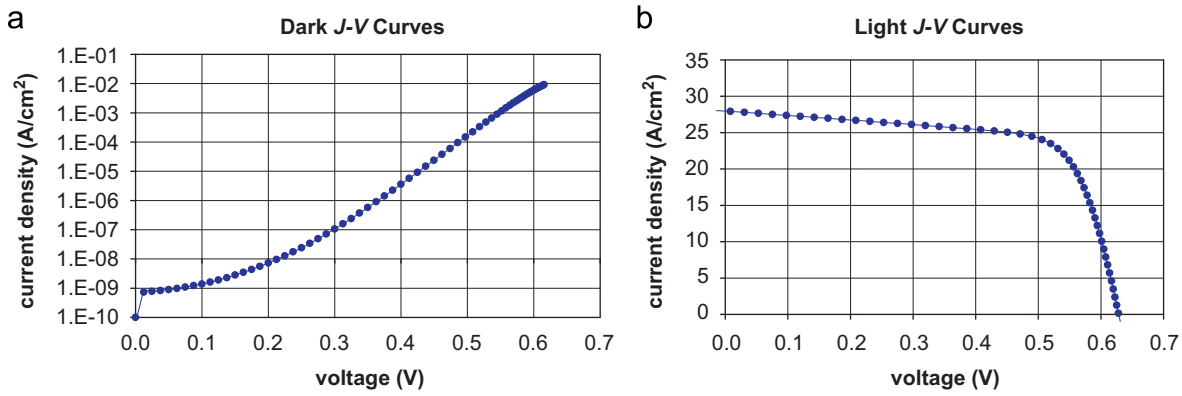

Fig. 7. (a) Dark *J–V* and (b) Light *J–V* curves of the equivalent circuit model in Fig. 6 by PC1D.

Since the *n*-type bulk generally has a high lifetime of over 1 ms, such Schottky contacts are linked to the p^+ layer at the rear through the *n*-type bulk and form a *p–n–p* transistor structure, as opposed to two isolated, back-to-back *p–n* diodes. Note that any metal contacting *n*-type surfaces would behave as a *p*-layer due to the band bending. Since the unusual shunting behavior is only present under illumination as observed in Fig. 4, the proposed transistor structure is of a phototransistor type, whereby its activation heavily depends on the presence of a light source to generate the base current that turns the transistor on. The phototransistor structure can be incorporated into the commonly used two-diode model for solar cells to provide a more accurate representation of the unusual shunting behavior, as observed in WFSF-6 and NFSF-1. As seen in Fig. 6, the *p*-type collector represents the Schottky contact of the copper onto the *n*-type bulk, which is referred to as the laser-induced defects in this case. Meanwhile, the *p*-type emitter corresponds to the p^+ layer formed by aluminum-alloying. The resistor R_H (the 'isolating resistor') represents the localized presence of the phototransistors. It isolates the phototransistor from the remaining good part of the cell. If there is sufficient light intensity to activate the phototransistor, the phototransistor circuitry would act like a short-circuit, connecting the phototransistor emitter to R_H. As a result, R_H would behave like R_{sh} and give rise to the previously observed shunting effect. These shunts become more pronounced particularly when R_H is small, i.e when the phototransistor is distributed all over the cell. In the dark, the phototransistor circuitry would act like an open-circuit, and hence any shunts associated with R_H would not occur. Fig. 7 shows that using the phototransistor model in Fig. 6, the unusual shunting behavior due to phototransistors can be well-explained. No shunts are apparent from the dark *J–V* curve (Fig. 7a), while strong linear shunts can be clearly observed from the light *J–V* curve (Fig. 7b).

3. Origin of phototransistor

In Section 2, it was seen the phototransistor occurs in the area where the nickel and copper did not plate onto the heavily laser-doped finger. Such occurrence is fairly uncommon as the selective plating technique allows metal ions to plate onto the exposed silicon surface, unless any dielectric layer is present on top as a plating barrier. Therefore, this section aims to further investigate the cause of such uneven plating that could lead to the formation of phototransistors.

3.1. Experimental details

Two batches of nine CZ, 1 Ω cm, ⟨1 0 0⟩ *n*-type silicon wafers were saw-damage-etched and textured, resulting in final wafer thickness of 180 μm. All wafers were processed according to the processing sequence outlined in Section 2. In Batch 1, the laser doping was carried out with a pulsing frequency of 100 kHz and a stage speed of 10 mm/s. In Batch 2, the laser doping was carried out with a pulsing frequency of 80 MHz and a faster stage speed of 2 m/s to achieve an approximately heavily doped region similar to

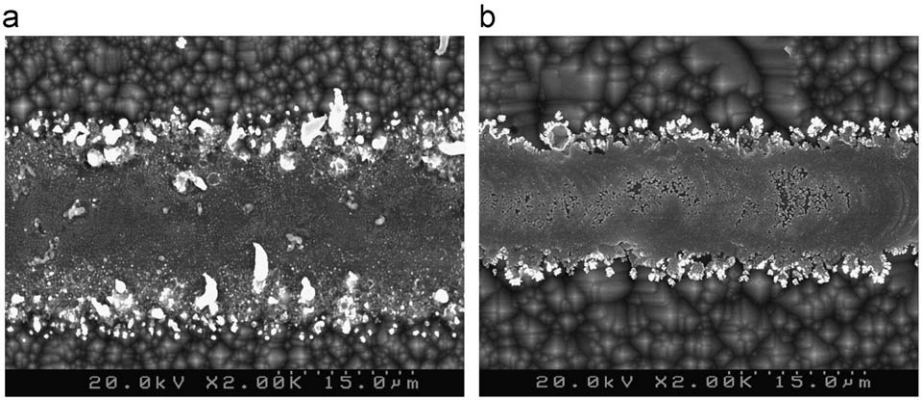

Fig. 8. Nickel light-induced plated fingers for (a) Batch 1 and (b) Batch 2.

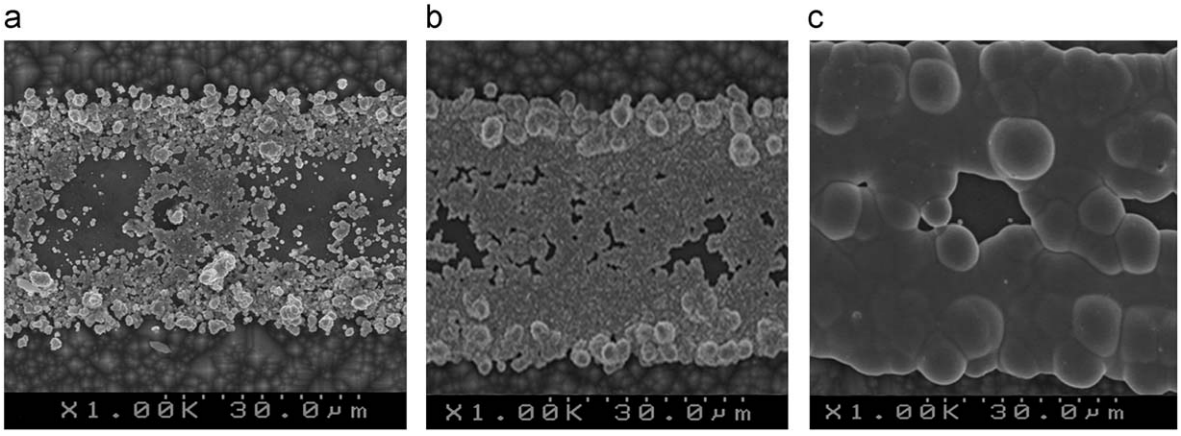

Fig. 9. Copper light-induced plated fingers for Batch 1 with varying plating time: (a) 1, (b) 5 and (c) 10 min.

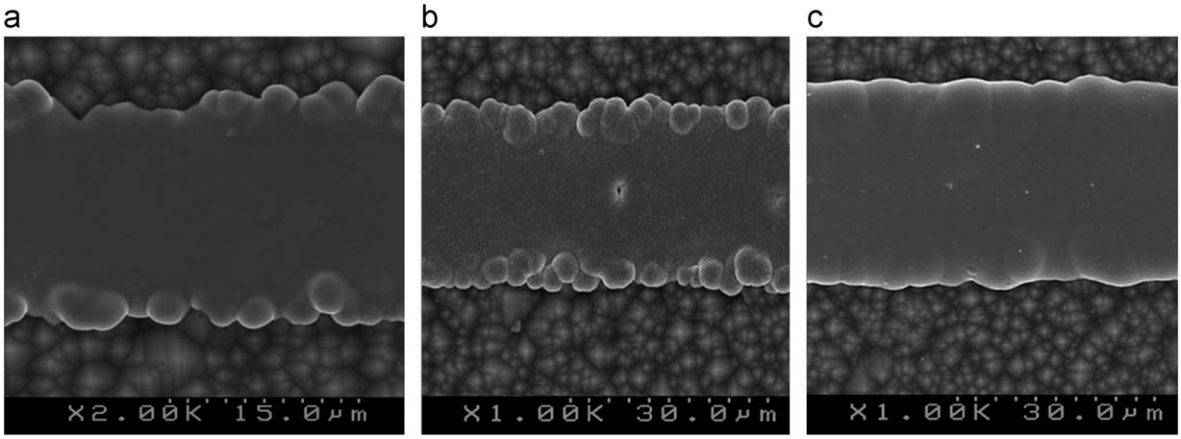

Fig. 10. Copper light-induced plated fingers for Batch 2 with varying plating time: (a) 1, (b) 5 and (c) 10 min.

that for Batch 1. Any residual spin-on-dopants and native oxide that might be present in the laser-doped lines were deglazed in HF 1% for 30 s prior to metallization. Each of the wafers from Batch 1 and 2 were then light-induced plated under the same plating conditions but with varying copper plating time: 15 s, 1, 5 and 10 min. Following the nickel/copper plating steps, the metal fingers in each sample were observed under optical microscope and Scanning Electron Microscope to study the progression of the LIP with time.

3.2. Results and discussions

In Batch 1, it can be seen from Fig. 8a that there is only a small number of nickel ions that plate onto the laser-doped finger. The plating also occurs in a non-uniform fashion along the finger. After 5 min of copper plating, some areas in the middle of the laser-doped region remain unplated while the copper plates at a significantly faster rate in the defected region adjacent to the finger (Fig. 9a and b). The copper from each side of the finger continues to grow in random directions and eventually merges, while some areas are still not plated (Fig. 9c). In contrast to Batch 1, the laser-doped fingers for Batch 2 are well-covered by nickel that appears light grey in Fig. 8b. In comparison with Batch 1, given the same amount of plating time, the copper plates more uniformly along the finger and progressively forms a smooth, semi-hemispherical copper line as shown in Fig. 10.

Running the laser at a very slow stage speed (10 mm/s) at a relatively high frequency (100 kHz) corresponds to a high percentage of overlaps between pulses, such that it can potentially keep the silicon molten for a long period of time at a very high temperature. At such a high temperature, there is possibility for the nitrogen atoms from the ambient and the scribed SiN_x dielectric layer to react with the molten silicon and form a thermally grown SiN_x layer. In this paper, the process of forming the thermally grown SiN_x layer will be referred to as "nitridation". Unlike Si–O bonds, Si–N bonds are less polarized. For this reason, SiN_x layers are more difficult to remove compared to native oxide (silicon dioxide) layers, for a given HF concentration in the deglazing step. As a result, this SiN_x layer is highly likely to inhibit the plating process.

It appears that nitridation is not always consistent along the laser-doped lines. This can be seen in Fig. 9 where the unplated areas are randomly distributed along the lines. In some cases, the thermally grown SiN_x layer might completely cover the laser-doped region, leaving the defects at either side of the finger as the only region for the nickel/copper to plate onto (Fig. 5b). Such a region introduces Schottky contacts that contribute to the formation of the phototransistor structure discussed in Section 2. Any light source used for the LIP could potentially activate the phototransistor, and as a result creates shunted regions with poor *FF*. It is worth noticing that the LIP technique relies heavily on the electrical properties of the cell, such as V_{oc} and *FF*, to achieve uniform plating. Once the phototransistor is on, it would be difficult for the metal to continue to plate onto such regions despite increasing plating time. As the plating proceeds, the copper balls do not increase in size while the middle part of the laser-doped region is still left unplated (Fig. 5b).

In the case where the thermally grown SiN_x layer covers only a small fraction of the laser-doped region, the copper is still able to plate well onto the entire surface of the heavily doped region. As a result, the phototransistor does not come into effect. Faster stage speed (2 m/s) as used for Batch 2 also appears to avoid the formation of such thermally grown SiN_x layer although the sheet resistance of the laser-doped region would not be as low.

It is also worth noticing that in the absence of surface coating by nitridation, LIP could also be ineffective at plating the regions in the vicinity of the phototransistors. This is because the shunting caused by the activation of the transistors would have naturally reduced the voltage required to drive the plating process.

4. Impacts of the phototransistors on cell performance

4.1. Experimental details

This section aims to study the impacts of phototransistors on the cell performance in terms of *FF*, V_{oc} and J_{sc}. To aid this study, NFSF-1 was cut with a laser to remove regions with phototransistors for comparison purposes. The DLIT imaging of this cell confirms that the cell area is free of any shunting due to the phototransistor effect (Fig. 11). The three cells used in this study, namely WFSF-6, NFSF-1 and NFSF-1 Cut, were characterized using light *J–V* and *Suns–*V_{oc} measurements. The results are shown in Table 1.

4.2. Results and discussions

4.2.1. Impact on FF

Similar to the case of the typical linear shunts caused by the metal wrap around at the cell edges, the presence of the shunts introduced by phototransistors under illumination has significantly pulled the *FF* down potentially from 75.1% to 63.8% for NFSF-1 (Table 1).

However, it is interesting to see that the *FF* obtained from the *Suns–*V_{oc} measurement remains high at 84.6% and 83.6% for WFSF-6 and NFSF-1 despite the shunting effect. Such a large difference

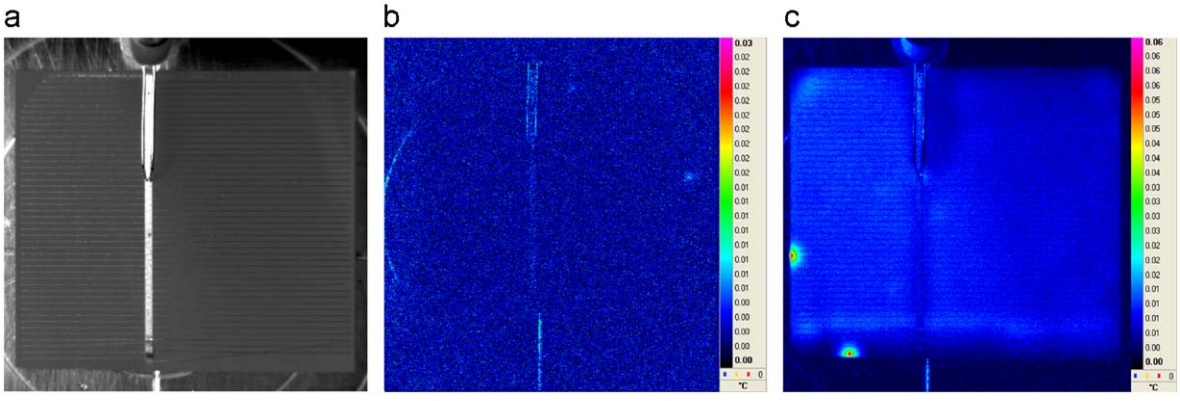

Fig. 11. Different LIT images for NFSF-1 cut: (a) camera image, (b) dark LIT image and (c) LIT image under steady-state illumination of a halogen light source at ~0.3 Suns. Images were taken at $f = 18$ Hz and $V_{RB} = -2$ V.

in *FF* between the *Suns–V_{oc}* measurement and the light *J–V* measurement could have been misinterpreted merely due to the high series resistance in the cells. In fact, the unusual shunting behavior due to the phototransistor appears to be undetected by the *Suns–V_{oc}* tester. A possible explanation might be that the *Suns–V_{oc}* tester uses a flash tester, whereby the light intensity continuously decays with a time constant of 1/e. In the case of the light *J–V* measurement, however, the cell is placed under steady-state illumination. Hence, towards the sampling of the lower voltage data points, there might not be sufficient amount of light from the flash tester to activate the phototransistor and to introduce shunts. Another possibility to explain the difference in the *FF* could be due to a fast sampling interval in the *Suns–V_{oc}* measurement of 0.1 ms between each data point. This causes insufficient amount of time for the light generated carries to diffuse through the base and be collected by the phototransistor collector. Therefore, the phototransistor appears to be inactive when the sampling occurs.

4.2.2. Impact on V_{oc}

As seen in Table 1, the phototransistors appear to have a slight impact on the cell V_{oc}. Any metal that contacts the exposed *n*-type substrate (defects) at either side of the laser-doped region and hence form a phototransistor, is believed to introduce areas with high recombinations, resulting in higher dark saturation current density J_{01} and lower V_{oc}. Therefore, reducing the cell area that contains phototransistors causes the V_{oc} to slightly increase from 623.9 mV (NFSF-1) to 625.8 mV (NFSF-1 Cut).

4.2.3. Impact on J_{sc}

With the aid of the shading mask, light *J–V* measurements were locally performed in four different parts of the cells: top left, top right, bottom left and bottom right with reference to Figs. 4 and 11. The localized *J–V* curves were plotted and compared (Fig. 12) to illustrate the impact of the phototransistors on J_{sc}.

For WFSF-6 (with an FSF), the *J–V* curves shown in Fig. 12a are consistent with the LIT image in Fig. 4c, whereby the phototransistor exists only in the top half of the cell. The presence of the phototransistor in these regions reduces the J_{sc} to below 30 mA/cm^2; whereas the J_{sc} of the remaining good areas at the bottom half of the cell generate J_{sc} of approximately 35 mA/cm^2. The *J–V* curves for NFSF-1 Cut as shown in Fig. 12b is also in agreement with the LIT image in Fig. 11c, whereby no (or little) shunting of the cells due to phototransistor is observed. The J_{sc} of this cell ranges from 29.4 to 32.8 mA/cm^2.

To confirm the J_{sc} values obtained from the *J–V* measurements, external quantum efficiency (EQE) measurements were performed on the four different parts of the cell: top left, top right, bottom left and bottom right. A shading mask with a 1 cm × 1 cm opening was used to avoid any stray light from impinging onto the cell. The J_{sc} values were extracted from the EQE graphs, as summarized in Table 2.

Since the EQE measurement was carried out relatively in the dark, any phototransistors that are present should remain inactivate. Hence, the extracted J_{sc} values for a particular region in the cell would represent the J_{sc} that can be achieved without any influence from the phototransistor effect. As seen in Table 2, J_{sc} of 34.8 and 33.3 mA/cm^2 are achievable for WFSF-6 (with an FSF) and NFSF-1 Cut (without an FSF), respectively. Such values are in good agreement with the J_{sc} values obtained in the light *J–V* measurements, as shown in Fig.12. Any discrepancies between the light *J–V* and the EQE measurements would be because the measurements might have not been carried out in the exact same spot. This is possible as the effective allowable area for the EQE measurement is restricted to 1 cm^2 while the *J–V* measurements allow a wider coverage of the cell surface.

Based on the *J–V* and the EQE measurements above, it can be seen that the presence of the phototransistors can cause a significant drop in J_{sc} when the cell operates under illumination. Provided that R_H in Fig. 6 is sufficiently small, it is suspected that

Table 1
Light *J–V* and *Suns–V_{oc}* data for WFSF-6, NFSF-1 and NFSF-1 Cut.

	WFSF-6[a]	NFSF-1[a]	NFSF-1 Cut
Light J–V measurement			
V_{oc} (mV)	629.4	623.9	625.8
J_{sc} (mA/cm^2)	27.9	28.5	30.2
FF (%)	68.7	63.8	75.1
Efficiency (%)	12.1	11.4	14.2
Suns–V_{oc} measurement			
V_{oc} (mV)	631.3	620.8	–
FF	84.6	83.6	–

[a] Cell with pronounced phototransistor effect.

Table 2
J_{sc} values for WFSF-6 and NFSF-1 Cut based on EQE measurements.

	J_{sc} (mA/cm^2)			
	Top left	Top right	Bottom left	Bottom right
WFSF-6	34.4	34.8	34.6	33.1
NFSF-1 cut	32.8	28.9	32.7	33.3

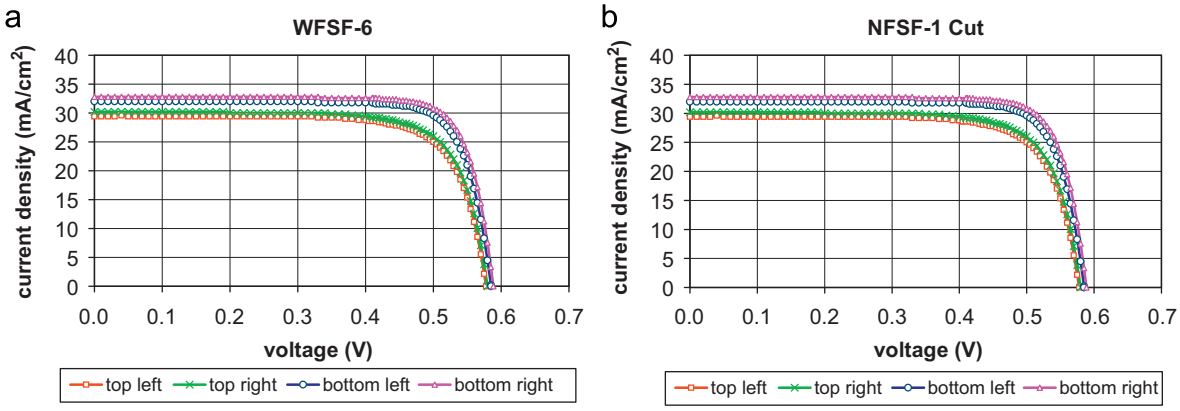

Fig. 12. *J–V* curves for different areas on the cell: (a) WFSF-6 (with an FSF) and (b) NFSF-1 cut (without an FSF).

the light generated carriers that are generated in the vicinity of plated defects (regions with phototransistors) would be used to activate the phototransistor rather than to contribute to the short-circuit current. Hence, the measured J_{sc} is always less than the actual J_{sc} that can be potentially achieved by the cell in the absence of the phototransistors.

5. Conclusions

In conclusion, we have provided strong evidence that the unusual shunting behavior, which only occurs under illumination, can exist in laser-doped *n*-type rear junction cells which have light-induced plated front contacts. It is found that phototransistors occur in areas in which metal plates only onto the defects adjacent to the laser-doped finger. The metal–silicon contact in these regions forms a Schottky contact which, combined with the rear aluminum-alloyed p^+ layer, results in the phototransistor structure. The activation of the phototransistors occurs under steady-state illumination, and introduces linear shunts that inhibit plating at the regions in the vicinity of the phototransistors. It appears that the decaying flash tester used in the *Suns*–V_{oc} measurement does not provide a sufficient amount of light to activate the phototransistors, so that the unusual shunting effect could not be detected.

It is shown that the presence of the phototransistor only reduces the V_{oc} by less than 5 mV, while the *FF* is significantly affected by the shunts and potentially dropping from 75% down to 64–69%. It is also interesting that with a phototransistor, the cell J_{sc} is suppressed to below 30 mA/cm^2. In the absence of phototransistor, the J_{sc} can potentially reach up to 35 and 33 mA/cm^2 for cells with an FSF and without an FSF, respectively, assuming that there are no further optimizations on the other cell properties. In this work, the limitations imposed on the cell V_{oc}, *FF* and J_{sc} have prevented the cell efficiency from exceeding 11.4% for cells without an FSF and 12.1% for cells with an FSF. By avoiding the formation of phototransistor structures in the first place, cell efficiency of at least 16.5% could be easily achieved.

Acknowledgements

This work was produced with the financial assistance of the Australian Research Council under the ARC Centre of Excellence Scheme and Suntech Power. The authors would like to thank Jürgen Weber for his assistance in the lock-in thermography imaging, and Alison Lennon for fruitful discussions.

References

[1] K Schmidt, A.G. Aberle, R. Hezel, Investigation of carrier lifetime instabilities in CZ grown silicon, in: Proceedings of the 26th IEEE Photovoltaic Specialists Conference, 29 Sep–3 October 1997, Anaheim, CA, USA, pp. 13–18.

[2] J.E. Cotter, J.H. Guo, P.J. Cousins, M.D. Abbott, F.W. Chen, K.C. Fisher, P-type versus n-type silicon wafers: prospects for high-efficiency commercial silicon solar cells, IEEE Trans. Electron Devices 53 (2006) 1893–1901.

[3] V.D. Mihailetchi, D.S. Sainova, L.J. Geerligs, A.W. Weeber, 17.4% efficiency solar cells on large area and thin n-type silicon with screen-printed aluminum-alloyed rear emitter, in: Proceedings of the 22nd European Photovoltaic Solar Energy Conference, 22–26 October 2007, Milan, Italy, pp. 837–840.

[4] C. Schmiga, H. Nagel, J. Schmidt, 19% efficient n-type czochralski silicon solar cells with screen-printed aluminum-alloyed rear emitter, Prog. Photovolt. Res. Appl. 14 (2006) 533–539.

[5] S.R. Wenham, M.A. Green, Self aligning method for forming a selective emitter and metallization in a solar cell, US Patent Application 2002/6429037.

[6] B.S. Tjahjono, L. Mai, Z. Hameiri, A. Sugianto, S. Wang, J.H. Guo, S.R. Wenham, High efficiency solar cell structures through the use of laser doping, in: Proceedings of the 22nd European Photovoltaic Solar Energy Conference, 22–26 October 2007, Milan, Italy, pp. 966–969.

[7] L. Mai, B.S. Tjahjono, A. Sugianto, M.E. Edwards, S.R. Wenham, Rear junction laser doped cells on CZ n-type silicon, in: Proceedings of the 18th International Photovoltaic Science and Engineering Conference, 19–23 January 2009, Kolkata, India.

[8] F.L. Durkee, Method of plating by means of light, US Patent Application 1979/4144139.

[9] A. Sugianto, B.S. Tjahjono, J.H. Guo, S.R. Wenham, Impact of laser-induced defects on the performance of solar cells using localized laser-doped regions beneath the metal contacts, in: Proceedings of the 22nd European Photovoltaic Solar Energy Conference, 22–26 October 2007, Milan, Italy, pp. 1759–1762.

[10] O. Breitenstein, J.P. Rakotoniaina, Unusual lock-in thermography signals: schottky-type grid contacts, peltier effects and thermal wave interference, in: Proceedings of the 4th IEEE World Conference on Photovoltaic Solar Energy Conference, 8–12 May 2006, Waikoloa, Hawaii, pp. 912–915.

[11] A.G Aberle, S.R. Wenham, M.A. Green, A new method for accurate measurements of the lumped series resistance of solar cells, in: Conference Record of the 23rd IEEE Photovoltaic Specialists Conference, May 1993, Louisville, KY, USA, pp. 133–139.

[12] M.C.A. Garcia, W. Herrmann, W. Bömer, B. Proisy, Thermal and electrical effects caused by outdoor hot-spot testing in associations of photovoltaic cells, Prog. Photovolt. Res. Appl. 11 (2003) 293–307.

[13] A Sugianto, Development and analysis of laser-doped solar cells, Undergraduate Thesis, The University of New South Wales, Sydney, 2007.